Design and optimization of liquid core optical ring resonator for refractive index sensing

Nai Lin,[1] Lan Jiang,[1,2,*] Sumei Wang,[1] Hai Xiao,[2] Yongfeng Lu,[3] and Hai-Lung Tsai[4]

[1]Laser Micro/Nano Fabrication Laboratory, School of Mechanical Engineering, Beijing Institute of Technology, 100081, Beijing, China

[2]Department of Electrical and Computer Engineering, Missouri University of Science and Technology, Rolla, Missouri 65409, USA

[3]Department of Electrical Engineering, University of Nebraska-Lincoln, Lincoln, Nebraska 68588-0511, USA

[4]Department of Mechanical and Aerospace Engineering, Missouri University of Science and Technology, Rolla, Missouri 65409, USA

*Corresponding author: jianglan@bit.edu.cn

Received 31 March 2011; revised 28 May 2011; accepted 28 May 2011; posted 31 May 2011 (Doc. ID 145089); published 7 July 2011

This study performs a detailed theoretical analysis of refractive index (RI) sensors based on whispering gallery modes (WGMs) in liquid core optical ring resonators (LCORRs). Both TE- and TM-polarized WGMs of various orders are considered. The analysis shows that WGMs of higher orders need thicker walls to achieve a near-zero thermal drift, but WGMs of different orders exhibit a similar RI sensing performance at the thermostable wall thicknesses. The RI detection limit is very low at the thermostable thickness. The theoretical predications should provide a general guidance in the development of LCORR-based thermostable RI sensors. © 2011 Optical Society of America

OCIS codes: 140.4780, 230.5750, 130.6010.

1. Introduction

Liquid core optical ring resonators (LCORRs) have recently attracted a good deal of attention in sensing applications [1–9]. In such resonators, the light propagates in the form of whispering gallery modes (WGMs) due to the total internal reflection of the light along the curved boundary between the high and low refractive index (RI) materials. The WGM is the surface mode, and its evanescent field extends into the low RI material. Consequently, LCORRs are sensitive to the RI change resulting from the change in the surrounding medium and binding of molecules to the resonator surface [5]. In addition, WGMs have high Q factors and thus provide an effective long interaction length between the light and the analytes [7]. This would significantly reduce the amount of sample needed for the detection compared to conventional waveguide-based sensors. Furthermore, LCORRs utilize thin-walled microtubes as fluidic channels to conduct samples and as ring resonators to detect analytes passing through the channel. Based on this unique structure, LCORRs can quickly deliver quantitative and kinetic information of samples without labeling [8]. Because of these distinctive advantages, LOCRRs represent a promising technology platform for RI sensing applications.

However, WGMs are susceptible to thermal fluctuations due to the environmental temperature variations and probe-induced energy absorptions. Especially for RI sensors with high Q factors, the instability of WGMs due to temperature-induced fluctuations significantly impairs the sensor performance [10]. In the case of the LOCRR, the thermal fluctuations cause changes in the refractive indices of both the LCORR wall material and the liquid solution. However, due to the negative thermal refraction

0003-6935/11/203615-07$15.00/0

of the liquid core, the resonance thermal drift can be reduced or even completely eliminated by adjusting the LCORR wall thickness [11]. The wall thickness also plays a significant role in determining the RI sensitivity and the Q factor (thus the RI detection limit) of LCORR-based RI sensors.

This study performs a detailed theoretical analysis of the thermal and RI sensing properties of WGM resonances in LCORRs. The numerical models to analyze the thermal drift, RI sensitivity, and detection limit are presented in Section 2. Based on the models, the influence of the LCORR wall thickness on RI sensing performance factors are studied in detail in Section 3. Both TE- and TM-polarized WGMs of various orders are considered. Major results are reported in Section 4.

2. Theory

A. WGMs in an LCORR

The general configuration of an LCORR structure is shown in Fig. 1. Over the years, WGM modal structures and resonance spectra of microresoantors have been widely studied [6,7,12]. For an LCORR, the WGM is characterized by a set of integers: m and l, which represent angular and radial mode numbers, respectively. Also, a WGM has two polarizations, TE mode and TM mode, with the magnetic field and the electric filed being along the cylinder longitudinal direction, respectively. Also, the two polarizations can be selectively excited by controlling the polarization of the coupling light. In general, the WGM resonance spectrum is determined by the size of the microresonator and the RI inside/outside the resonator. Considering an LCORR with the inner radius of R_1 and outer radius of R_2 [Fig. 1(b)], the characteristic equation to specify the resonant wavelengths λ_R of the WGMs can be expressed by [6,7]

$$N_0 \frac{H_m'^{(1)}(k_0 n_3 R_2)}{H_m^{(1)}(k_0 n_3 R_2)} = \frac{B_m J_m'(k_0 n_2 R_2) + H_m'^{(1)}(k_0 n_2 R_2)}{B_m J_m(k_0 n_2 R_2) + H_m^{(1)}(k_0 n_2 R_2)},$$
$$N_0 = \begin{cases} n_2/n_3, & \text{TE modes} \\ n_3/n_2, & \text{TM modes} \end{cases}, \quad (1)$$

where $k_0 = 2\pi/\lambda_R$ is the resonant wave vector; J_m and $H_m^{(1)}$ are the mth Bessel function and the mth Hankel function of the first kind, respectively; and B_m is a coefficient that is given by

$$B_m = \frac{N_1 J_m(k_0 n_1 R_1) H_m'^{(1)}(k_0 n_2 R_1) - J_m'(k_0 n_1 R_1) H_m^{(1)}(k_0 n_2 R_1)}{J_m'(k_0 n_1 R_1) J_m(k_0 n_2 R_1) - N_1 J_m(k_0 n_1 R_1) J_m'(k_0 n_2 R_1)}, \quad N_0 = \begin{cases} n_1/n_2, \text{TE modes} \\ n_2/n_1, \text{TM modes} \end{cases}. \quad (2)$$

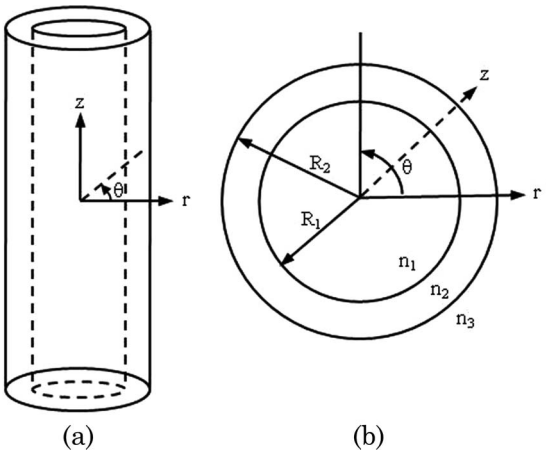

Fig. 1. Schematic structure of an LCORR with an inner radius of R_1 and outer radius of R_2. n_1, n_2, and n_3 are the refractive indices of the liquid core, ring wall, and surrounding medium, respectively.

For a given value of m, there are multiple values of λ_R that satisfy the characteristic equation. These resonant modes are called the first-order mode, the second-order mode …, and the lth-order mode in the decreasing value of λ_R.

B. Thermal Drift

For a given WGM mode, the resonant wavelength shift $\delta\lambda_R$ versus the temperature variation δT can be given by [13]

$$\frac{\delta\lambda_R}{\delta T} = \lambda_R \left(\frac{1}{n_{\text{eff}}} \frac{dn_{\text{eff}}}{dT} + \alpha \right), \quad (3)$$

where α is the linear thermal expansion coefficient of the LCORR and n_{eff} is the effective RI of the WGMs, which can be approximately expressed as $n_{\text{eff}} = \eta_1 n_1 + \eta_2 n_2 + \eta_3 n_3$. η_1, η_2, and η_3 denote the fractions of light energy distributed in the liquid core, the ring wall, and the surrounding medium, respectively. Thus, $\delta\lambda_R/\delta T$ is further expressed as

$$\frac{\delta\lambda_R}{\delta T} \approx \lambda_R \left(\frac{\sum_{i=1}^{3} \eta_i (dn_i/dT)}{\sum_{i=1}^{3} (\eta_i n_i)} + \alpha \right), \quad (4)$$

where dn_1/dT, dn_2/dT, and dn_3/dT are the thermal refraction coefficients of the liquid core, the wall, and the surrounding medium, respectively. The energy fractions can be calculated by

$$\eta_i = \frac{I_i}{I_1 + I_2 + I_3}, \qquad i = 1,2,3 \text{ (TE modes)}, \tag{5a}$$

$$\eta_i = \frac{n_i^2 I_i}{n_1^2 I_1 + n_2^2 I_2 + n_3^2 I_3}, \qquad i = 1,2,3 \text{ (TM modes)}, \tag{5b}$$

where

$$\begin{aligned} I_1 &= \int_0^{R_1} |A_m J_m(k_0 n_1 r)|^2 \mathrm{d}_r, \\ I_3 &= \int_{R_2}^{\infty} |C_m H_m^{(1)}(k_0 n_3 r)|^2 \mathrm{d}_r, \\ I_2 &= \int_{R_1}^{R_2} |B_m J_m(k_0 n_2 r) + H_m^{(1)}(k_0 n_2 r)|^2 \mathrm{d}_r. \end{aligned} \tag{5c}$$

A_m and C_m are the coefficients determined by

$$\begin{aligned} A_m &= \frac{B_m J_m(k_0 n_2 R_1) + H_m^{(1)}(k_0 n_2 R_1)}{J_m(k_0 n_1 R_1)}, \\ C_m &= \frac{B_m J_m(k_0 n_2 R_2) + H_m^{(1)}(k_0 n_2 R_2)}{H_m^{(1)}(k_0 n_3 R_2)}. \end{aligned} \tag{5d}$$

Substituting Eq. (5) into Eq. (4), the thermal drift for the TE and TM modes in the LCORRs can be respectively expressed by

$$\left(\frac{\delta\lambda_R}{\delta T}\right)_{\mathrm{TE}} \approx \lambda_R \left(\frac{\sum_{i=1}^3 I_i (dn_i/dT)}{\sum_{i=1}^3 (I_i n_i)} + \alpha\right), \tag{6a}$$

$$\left(\frac{\delta\lambda_R}{\delta T}\right)_{\mathrm{TM}} \approx \lambda_R \left(\frac{\sum_{i=1}^3 I_i n_i^2 (dn_i/dT)}{\sum_{i=1}^3 (I_i n_i^3)} + \alpha\right). \tag{6b}$$

C. RI Sensitivity

Considering an RI change of the liquid core δn_1, the resonant wavelength shift $\delta\lambda_R$ induced by δn_1 can be calculated by $\delta\lambda_R = \delta n_1 \times S$. S, the RI sensitivity, can be expressed by

$$S = \frac{\delta\lambda_R}{\delta n_1} = -\frac{\lambda_R}{\delta n_1} \cdot \frac{\delta k}{k_0}, \tag{7}$$

where δk is the wave vector shift induced by δn_1. If the RI change of the liquid core is uniform and $\delta(n_1^2) \ll 1$, the fractional shift $\delta k/k_0$ can be calculated using perturbation theory [14,15], which is given as

$$\left(\frac{\delta k}{k_0}\right)_{\mathrm{TE}} = -\frac{\delta(n_1^2)[T_0(R_1)T_0'(R_1^-) + n_1^2 k_0^2 I_1]}{2n_1^4 k_0^2 \sum_{i=1}^3 I_i}, \tag{8a}$$

TE modes,

$$\left(\frac{\delta k}{k_0}\right)_{\mathrm{TM}} = -\frac{\delta(n_1^2) I_1}{2\sum_{i=1}^3 n_i^2 I_i}, \qquad \text{TM modes}, \tag{8b}$$

where $T(r)$ is the function to describe the field distribution of WGMs along the radial direction, and T_0 denotes the field before the RI change; R_1^- is infinitesimally smaller than R_1. $T(r)$ is given by

$$T(r) = \begin{cases} A_m J_m(k_0 n_1 r) & r < R_1 \\ B_m J_m(k_0 n_2 r) + H_m^{(1)}(k_0 n_2 r) & R_1 < r < R_2 \\ C_m H_m^{(1)}(k_0 n_3 r) & r > R_2 \end{cases}. \tag{9}$$

Substituting Eqs. (8) and (9) into Eq. (7), and considering $\delta(n_1^2) \approx 2n_1 \delta n_1$ if $\delta(n_1^2) \ll 1$, the RI sensitivity for TE and TM modes of the LCORRs can be respectively expressed as

$$S_{\mathrm{TM}} = \frac{n_1 \lambda_R I_1}{\sum_{i=1}^3 n_i^2 I_i} = \frac{\lambda_R}{n_1}\eta_1, \tag{10a}$$

$$\begin{aligned} S_{\mathrm{TE}} &= \frac{\lambda_R^2 [k_0 n_1 I_1 + A_m^2 J_m(k_0 n_1 R_1) J_m'(k_0 n_1 R_1)]}{2\pi n_1^2 \sum_{i=1}^3 I_i} \\ &= \frac{\lambda_R}{n_1}\eta_1 + \frac{A_m^2 \lambda_R^2 J_m(k_0 n_1 R_1) J_m'(k_0 n_1 R_1)}{2\pi n_1^2 \sum_{i=1}^3 I_i}. \end{aligned} \tag{10b}$$

The unit of RI sensitivity is nanometers per RI unit (RIU).

D. Detection Limit

The detection limit (DL), defined as the smallest detectable change of the RI, is proportional to $1/(S \times Q)$ [16]. The Q factor is defined as the ratio of the resonant wavelength to the FWHM of the resonance. In practical applications of RI sensors, various noises can perturb the resonance spectrum. In these cases, the accurate detection of resonant wavelength shift is difficult for a broad resonance line width, which suggests that a narrow resonance (thus a high Q value) is preferred to achieve a good detection performance. The Q factor of the LCORR is determined by the lumped loss of light in the resonator, which includes the tunneling loss (also known as radiation loss), the scattering loss from surface irregularities, and the material absorption loss of light [6]. Tunneling loss is due to the curvature of the waveguiding boundaries in the direction of propagation, and it is very small for the microresonator with a large radius. Thus, the total Q factor of the LCORR can be further expressed as

$$\frac{1}{Q} \approx \frac{1}{Q_{\mathrm{sca}}} + \frac{1}{(Q_{\mathrm{abs}})_{\mathrm{wall}}} + \frac{1}{(Q_{\mathrm{abs}})_{\mathrm{core}}}, \tag{11}$$

where $1/Q_{\mathrm{sca}}$ denotes the scattering loss and $1/(Q_{\mathrm{abs}})_{\mathrm{wall}}$ and $1/(Q_{\mathrm{abs}})_{\mathrm{core}}$ denote the material absorption loss of light in the LCORR wall and liquid

core, respectively. $(Q_{abs})_{core}$ can be further calculated by $(Q_{abs})_{core} = 2\pi n_1/(\lambda_R \sigma \eta_1)$ [17], where σ is the optical attenuation coefficient of the liquid core.

3. Results and Discussion

In the case study, the values of the refractive indices are chosen as $n_2 = 1.45$ for the fused silica LCORR wall, $n_1 = 1.33$ for the liquid core (primarily composed of water), and $n_3 = 1.0$ for the air outside the LCORR. The thermal refraction coefficients of the liquid core and the silica wall are $dn_1/dT \approx -1.0 \times 10^{-4}/\mathrm{K}$ and $dn_2/dT \approx 6.4 \times 10^{-6}/\mathrm{K}$, respectively, and the linear thermal expansion coefficient of the LCORR is $\alpha \approx 5.0 \times 10^{-7}/\mathrm{K}$ at room temperature [11]. Figure 2 shows $\delta\lambda_R/\delta T$ for both TE and TM modes of the first three orders as a function of the wall thickness $h_0 (h_0 = R_2 - R_1)$. The outer radius of the LCORR is kept at $R_2 = 50\,\mu\mathrm{m}$ for all cases, and the angular mode numbers m are chosen to keep the resonant wavelength around 1550 nm. As shown in Fig. 2, the changes of $\delta\lambda_R/\delta T$ with h_0 are similar for the TE and TM modes. With the wall thickness increases, the light energy in the liquid core is gradually transferred into the silica wall. As a result, the positive thermal refraction of the silica wall becomes dominant and counteracts the negative thermal refraction of the liquid core, which finally leads to the change of $\delta\lambda_R/\delta T$ from negative to positive. A near-zero thermal drift can be achieved when $h_0 \approx 1.3$, 2.5, and $3.5\,\mu\mathrm{m}$ for the TM modes of $l = 1, 2, 3$, respectively. Also, the TE mode needs a slightly thicker silica wall to achieve the near-zero thermal drift compared to the TM mode of the same order. In the following discussion, the wall thickness at which the thermal drift is near-zero is referred to as the thermostable thickness.

Figure 3 shows the resonant wavelength shift as a function of the temperature change for the first-order TM mode at various wall thicknesses. The curves represent the approximate results evaluated by

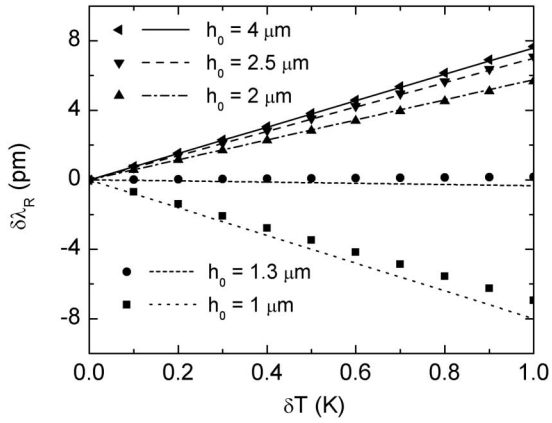

Fig. 3. Resonant wavelength shift $\delta\lambda_R$ as a function of the temperature change δT for the $\mathrm{TM}_{l=1}$ mode at various LCORR wall thicknesses.

$\delta\lambda_R = (\delta\lambda_R/\delta T) \times \delta T$. The symbols denote the accurate results of $\delta\lambda_R$ that are numerically calculated by substituting the temperature variation-induced size and RI changes into the resonance condition of Eq. (1). As shown in Fig. 3, the total resonance shift of the $\mathrm{TM}_{l=1}$ mode is about zero with the 1 K temperature change at $h_0 = 1.3\,\mu\mathrm{m}$. When $h_0 \geq 2.5\,\mu\mathrm{m}$, most of the light energy is inside the silica wall and the negative refraction effect of the liquid core is nearly completely eliminated, which finally induces a large redshift of the resonance. The results calculated by the model of Eq. (6) are basically identical with the discrete results by the resonance condition of Eq. (1).

The aforementioned analysis demonstrates that the thermal drift of the resonance can be reduced or even eliminated by controlling the wall thickness. But, for the LCORRs of different wall thicknesses, the RI sensitivities might also be quite different. Figure 4 shows the RI sensitivity for both TE and TM modes of the first three orders as a function of

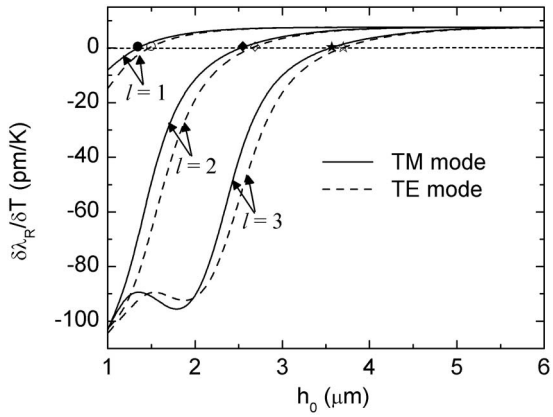

Fig. 2. $\delta\lambda_R/\delta T$ for TM modes (solid curves) and TE modes (dashed curves) of the first three orders as a function of the LCORR wall thickness h_0. The symbols denote $\delta\lambda_R/\delta T = 0$ for the $\mathrm{TM}_{l=1}$ (filled cirlces), $\mathrm{TE}_{l=1}$ (open circles), $\mathrm{TM}_{l=2}$ (filled diamonds), $\mathrm{TE}_{l=2}$ (open diamonds), $\mathrm{TM}_{l=3}$ (filled stars), and $\mathrm{TE}_{l=3}$ (open stars) modes, respectively.

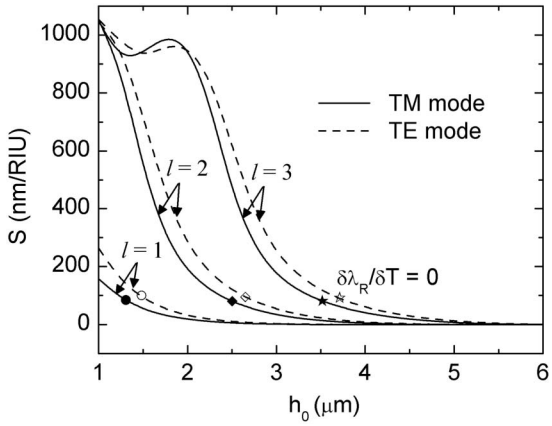

Fig. 4. RI sensitivity S for TM modes (solid curves) and TE modes (dashed curves) of the first three orders as a function of the LCORR wall thickness h_0. The symbols denote $\delta\lambda_R/\delta T = 0$ for the $\mathrm{TM}_{l=1}$ (filled circles), $\mathrm{TE}_{l=1}$ (open circles), $\mathrm{TM}_{l=2}$ (filled diamonds), $\mathrm{TE}_{l=2}$ (open diamonds), $\mathrm{TM}_{l=3}$ (filled stars), and $\mathrm{TE}_{l=3}$ (open stars) modes, respectively.

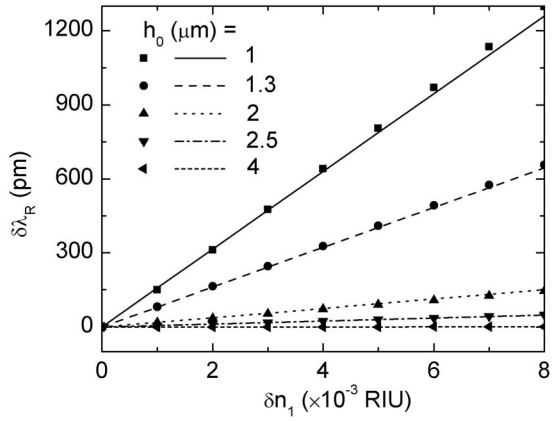

Fig. 5. Resonant wavelength shift $\delta\lambda_R$ as a function of the RI change δn_1 for the $TM_{l=1}$ mode at various LCORR wall thicknesses.

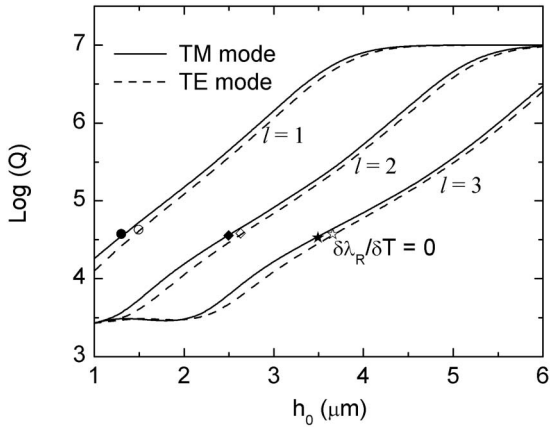

Fig. 6. Q factors for TM modes (solid curves) and TE modes (dashed curves) of the first three orders as a function of the LCORR wall thickness h_0. The symbols denote $\delta\lambda_R/\delta T = 0$ for the $TM_{l=1}$ (filled circles), $TE_{l=1}$ (open circles), $TM_{l=2}$ (filled diamonds), $TE_{l=2}$ (open diamonds), $TM_{l=3}$ (filled stars), and $TE_{l=3}$ (open stars) modes, respectively.

the wall thickness. At $h_0 = 1\,\mu$m, the RI sensitivities are about 157, 1053, and 1049 nm/RIU for the TM modes of $l = 1, 2, 3$, respectively. Also, the RI sensitivity of the TE mode is slightly larger than that of the TM mode of the same order. As the wall thickness increases, the light energy in the liquid core is reduced and thus leads to a reduction in RI sensitivity. From Fig. 4, at the thermostable thicknesses, the RI sensitivities for WGMs of the same polarization but different orders are almost identical. For the TM and TE modes, the RI sensitivities are about 83 and 90 nm/RIU, respectively, at the thermostable thicknesses, which are much smaller than the sensitivities at $h_0 = 1\,\mu$m. Figure 5 shows the resonant wavelength shift as a function of the RI change of the liquid core for the $TM_{l=1}$ mode at various wall thicknesses. The curves represent the approximate results evaluated by $\delta\lambda_R = S \times \delta n_1$. The symbols denote the accurate results of $\delta\lambda_R$ that are numerically calculated by substituting δn_1 into the resonance condition of Eq. (1). It is shown that the LCORRs exhibit an excellent linear sensing characteristic at various wall thicknesses. Also, the curves are in agreement with the accurate values in the range of refractive changes.

The LCORR of a smaller wall thickness has a higher RI sensitivity, but a smaller Q factor, as shown in Fig. 6. The Q factor determined by the scattering and absorption loss of the ring wall is taken to be around 10^7 [6], and the optical attenuation coefficient of water at the wavelength around 1550 nm is about $2.2 \times 10^3\ \mathrm{m}^{-1}$ [18]. As the wall thickness decreases, more light energy distributes inside the liquid core, and the Q factor is significantly decreased due to the large absorption loss of light in the liquid core. For instance, at $h_0 = 1\,\mu$m, the Q factors are as low as 1.8×10^4, 2.7×10^3, and 2.7×10^3 for the TM modes of $l = 1, 2, 3$, respectively. For the same wall thickness, the Q factor of the TE mode is slightly lower than that of the TM mode of the same order. At the thermostable thicknesses, the Q factors are similar for the WGMs of different orders, which are about 3.5×10^4 and 4×10^4 for the TM and TE modes, respectively. Figure 7 shows $1/(S \times Q)$ for both TE and TM modes of the first three orders as a function of the wall thickness. When the ring wall is thin enough, the Q factor is mainly limited by the large absorption loss in the liquid core, and $1/(S \times Q)$ for the TM mode can be further approximated by

$$\frac{1}{S_{\mathrm{TM}} \times Q} \approx \frac{n_1}{\eta_1 \lambda_R} \times \frac{\eta_1 \lambda_R \sigma}{2\pi n_1} = \frac{\sigma}{2\pi}. \tag{12}$$

So, in a thin-walled LCORR, the detection limits are almost identical for the TM-polarized WGMs of different orders. Figure 7 also shows that the TE mode has a smaller detection limit compared with the TM mode of the same order. However, if the ring wall thickness exceeds a certain value, the detection limits of both TE and TM modes increase significantly with the wall thickness. For instance, to

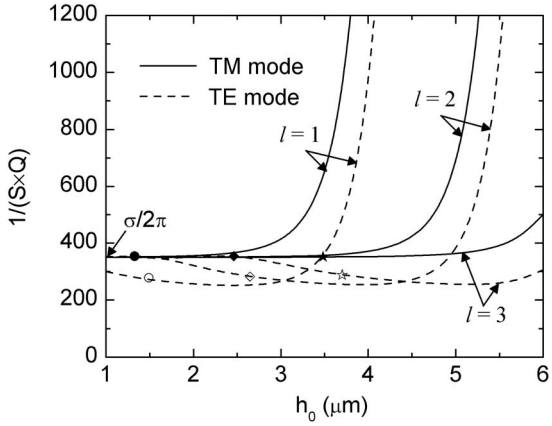

Fig. 7. $1/(S \times Q)$ for TM modes (solid curves) and TE modes (dashed curves) of the first three orders as a function of the LCORR wall thickness h_0. The symbols denote $\delta\lambda_R/\delta T = 0$ for the $TM_{l=1}$ (filled circles), $TE_{l=1}$ (open circles), $TM_{l=2}$ (filled diamonds), $TE_{l=2}$ (open diamonds), $TM_{l=3}$ (filled stars), and $TE_{l=3}$ (open stars) modes, respectively.

ensure a low detection limit, the wall thickness should be smaller than 3 μm for the first-order WGM.

To further illustrate the influence of temperature fluctuations on the detection limit, a detection system with a resolution of 1/100th of the resonance linewidth is considered. According to Fig. 6, when $h_0 < 3\,\mu$m, the Q factors of all modes are smaller than $\sim 10^6$. As for such low Q factors, the wavelength resolution of 1/100th of the resonance linewidth can be achieved with ease [19]. Then, the detection limit can be further evaluated by

$$\mathrm{DL} \approx \frac{\lambda_R}{100} \times \frac{1}{S \times Q} + \left(\frac{\delta \lambda_R}{\delta T}\right) \times \frac{\delta T}{S}. \qquad (13)$$

The second part of right side of Eq. (13) corresponds to the detection limit determined by the thermal drift. Figure 8 shows the detection limit of the first-order WGMs in the range of wall thicknesses from 1 to 3 μm for a temperature fluctuation of $\delta T = 0$, 0.05, 0.5, and 1 K, respectively. Without temperature fluctuation (i.e., $\delta T = 0$ K), the detection limits at $\lambda_R \approx 1550$ nm are as low as $\sim 5.5 \times 10^{-6}$ and $\sim 4 \times 10^{-6}$ RIU for the TM and TE modes, respectively. However, as the temperature fluctuation increases, the detection limit might be significantly impaired. For example, for the temperature fluctuation of $\delta T = 0.5$ K, the detection limit of the first-order TM mode is $\sim 2.2 \times 10^{-3}$ RIU at $h_0 = 3\,\mu$m, which is about three orders of magnitude larger than that without temperature fluctuation. However, it is also shown that the detection limit at the thermostable wall thickness is unaffected and remains very small under large temperature fluctuations. So, the ring wall thickness should be optimized to be around the thermostable thickness to ensure a near-zero thermal drift of the resonance.

As the water absorption loss of light in the visible range is almost three orders of magnitude smaller than that in the near-IR range [18], the Q factor might be greatly improved by choosing the resonant wavelength in the visible range as the detection wavelength. For example, at $\lambda_R \approx 780$ nm, the optical attenuation coefficient of water is $\sigma = \sim 3\,\mathrm{m}^{-1}$, and the Q factors for the WGMs of the first three orders are larger than 3×10^6 at $h_0 > 1\,\mu$m. As for such high Q factors, the detection limit is further restricted by the linewidth of the coupling laser [10]. Figure 9(a) shows the detection limit for both TM and TE modes of the first three orders at $\lambda_R \approx 780$ nm and $\delta T = 0$ K, considering the laser linewidth of 10 fm [20]. It is shown that the smallest detection limit at $\lambda_R \approx 780$ nm can reach $\sim 2 \times 10^{-8}$ RIU if there is no temperature fluctuation. However, in practical applications of the LCORRs, it is difficult to achieve a thermal stability close to 0 K. Also, the temperature fluctuation significantly impairs the detection limit unless the wall thickness is optimized to be around the thermostable wall thickness, as shown in Fig. 9(b). At the thermostable thickness, the detection limit of $\lambda_R \approx 780$ nm is about 3×10^{-7} RIU, which is more than one order of magnitude lower than that of $\lambda_R \approx 1550$ nm. For the WGM of the same order, the thermostable thickness is smaller for a shorter detection wavelength. For instance, for the third-order TM mode, the thermostable thicknesses are about 1.9 and 3.5 μm at $\lambda_R \approx 780$ and 1550 nm, respectively.

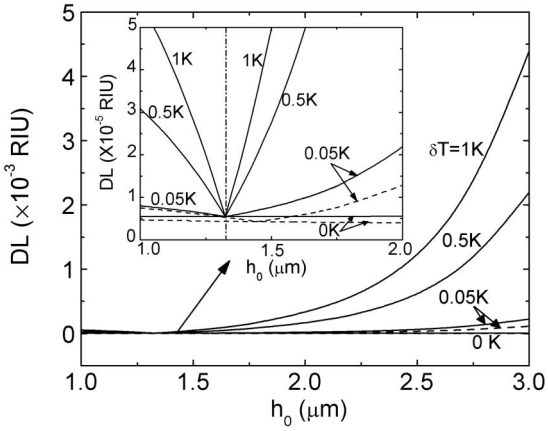

Fig. 8. Detection limit of the first-order TM mode (solid curves) and first-order TE mode (dashed curves) as a function of the LCORR wall thickness h_0 for a temperature fluctuation of $\delta T = 0$, 0.05, 0.5, and 1 K, respectively.

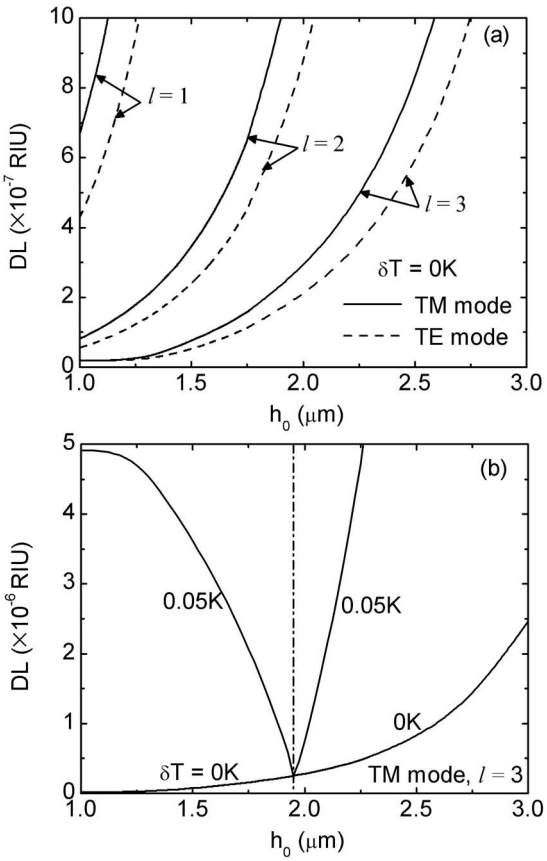

Fig. 9. Detection limit at $\lambda_R \approx 780$ nm as a function of the wall thickness h_0 (a) for the WGMs of the first three orders at $\delta T = 0$ K and (b) for the third-order TM mode at $\delta T = 0$ and 0.05 K, respectively.

4. Conclusions

The thermal and RI sensing responses of WGMs in LCORRs are theoretically investigated, using the numerical models derived in this study. It is shown that WGMs of higher orders need larger wall thicknesses to achieve the near-zero thermal drift, and the thermostable thickness for the TE mode is slightly larger than that of the TM mode of the same order. LCORRs exhibit an excellent linear RI sensing characteristic at various wall thicknesses, and the results of the models derived in this study agree well with the accurate numerical results. Further analysis shows that the detection limits are very low at the thermostable thicknesses, which can be obtained on the order of 10^{-6} and 10^{-7} RIU at $\lambda_R \approx 1550$ and 780 nm, respectively, without any temperature control. The predications of our models can guide the design and optimization of LCORR-based RI sensors.

This research is supported by the National Natural Science Foundation of China (NSFC) (grants 90923039 and 51025521) and the 111 Project of China (grant B08043).

References

1. I. M. White, H. Oveys, and X. Fan, "Liquid-core optical ring-resonator sensors," Opt. Lett. **31**, 1319–1321 (2006).
2. I. M. White, H. Oveys, X. Fan, T. L. Smith, and J. Zhang, "Integrated multiplexed biosensors based on liquid core optical ring resonators and antiresonant reflecting optical waveguides," Appl. Phys. Lett. **89**, 191106 (2006).
3. I. M. White, H. Zhu, J. D. Suter, N. M. Hanumegowda, H. Oveys, M. Zourob, and X. Fan, "Refractometric sensors for lab-on-a-chip based on optical ring resonators," IEEE Sens. J. **7**, 28–35 (2007).
4. H. Zhu, I. M. White, J. D. Suter, P. S. Dale, and X. Fan, "Analysis of biomolecule detection with optofluidic ring resonator sensors," Opt. Express **15**, 9139–9146 (2007).
5. V. Zamora, A. Díez, M. V. Andrés, and B. Gimeno, "Refractometric sensors based on whispering-gallery modes of thin capillaries," Opt. Express **15**, 12011–12016 (2007).
6. T. Ling and L. J. Guo, "A unique resonance mode observed in a prism-coupled micro-tube resonator sensor with superior index sensitivity," Opt. Express **15**, 17424–17432 (2007).
7. T. Ling and L. J. Guo, "Analysis of the sensing properties of silica microtube resonator sensors," J. Opt. Soc. Am. B **26**, 471–477 (2009).
8. Y. Sun and X. Fan, "Analysis of ring resonators for chemical vapor sensor development," Opt. Express **16**, 10254–10268 (2008).
9. H. Li, Y. Guo, Y. Sun, K. Reddy, and X. Fan, "Analysis of single nanoparticle detection by using 3-dimensionally confined optofluidic ring resonators," Opt. Express **18**, 25081–25088 (2010).
10. I. M. White and X. Fan, "On the performance quantification of resonant refractive index sensors," Opt. Express **16**, 1020–1028 (2008).
11. J. D. Suter, I. M. White, H. Zhu, and X. Fan, "Thermal characterization of liquid core optical ring resonator sensors," Appl. Opt. **46**, 389–396 (2007).
12. C. F. Bohren and D. R. Huffman, *Absorption and Scattering of Light by Small Particles* (Wiley, 1998).
13. B. B. Li, Q. Y. Wang, Y. F. Xiao, X. F. Jiang, Y. Li, L. X. Xiao, and Q. H. Cong, "On chip, high-sensitivity thermal sensor based on high-Q polydimethylsiloxane-coated microresonator," Appl. Phys. Lett. **96**, 251109 (2010).
14. I. Teraoka and S. Arnold, "Enhancing the sensitivity of a whispering-gallery mode microsphere sensor by a high-refractive-index surface layer," J. Opt. Soc. Am. B **23**, 1434–1442 (2006).
15. I. Teraoka and S. Arnold, "Whispering-gallery modes in a microsphere coated with a high-refractive index layer: polarization-dependent sensitivity enhancement of the resonance-shift sensor and TE-TM resonance matching," J. Opt. Soc. Am. B **24**, 653–659 (2007).
16. C. Y. Chao and L. J. Guo, "Design and optimization of microring resonators in biochemical sensing applications," J. Lightwave Technol. **24**, 1395–1402 (2006).
17. M. L. Corodetsky, A. A. Savchenkov, and V. S. Ilchenko, "Ultimate Q of optical microsphere resonators," Opt. Lett. **21**, 453–455 (1996).
18. G. M. Hale and M. R. Querry, "Optical constants of water in the 200 nm to 200 μm wavelength region," Appl. Opt. **12**, 555–563 (1973).
19. F. Vollmer and S. Arnord, "Whispering-gallery-mode biosensing: label-free detection down to single molecules," Nat. Methods **5**, 591–596 (2008).
20. N. M. Hanumegowda, C. J. Stica, B. C. Patel, I. M. White, and X. Fan, "Refractometric sensors based on microsphere resonators," Appl. Phys. Lett. **87**, 201107 (2005).